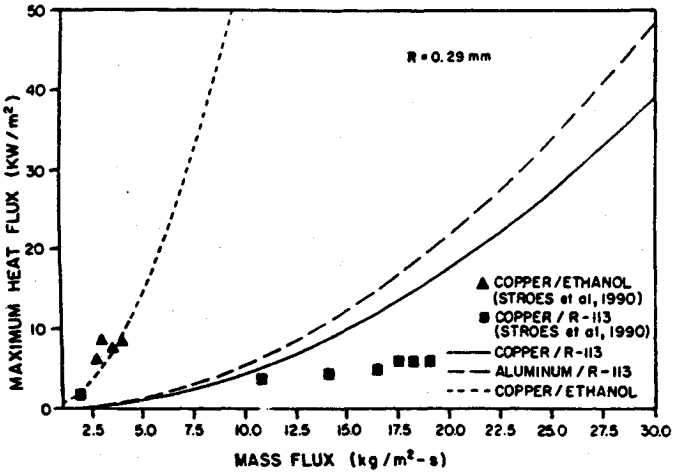

Fig. 2 Comparison of experimental and predicted values for a grooved plate, R = 0.29 mm.

Writing the liquid velocity U in terms of the mass flux G, Eqs. (8) and (10) can be rewritten as

$$U_w = \frac{1}{2}\left[\left(\frac{G}{\rho_l}\right) + \sqrt{\left(\frac{G}{\rho_l}\right)^2 - \frac{16q''\alpha}{\pi R\rho_l h_f}}\right] \tag{13}$$

$$q_{\max} = \frac{\pi R\rho_l h_f}{16\alpha\rho_l} G^2 \tag{14}$$

Therefore, for a given mass flux and groove radius, the rewetting heat flux can not exceed the value described by Eq. (10), otherwise the liquid supplied will be unable to provide sufficient cooling to allow the surface to rewet. It is also apparent from Eq. (10) that $q''_{\max}$ is a function of the thermal properties of both the liquid and the heated plate and also of the mass flux, proposed but not verified by Iloeje et al.[4]

It is worthy to note that Eqs. (8) and (10) are for a given mass flux. If the liquid flowing in the grooves is driven only by capillary pressure or surface tension, as is the case in heat pipes and capillary pumped loops, the liquid mass flux or velocity can be found from the transport equations and determined as a function of the capillary pressure difference caused by the groove radius. In this type of situation, the rewetting velocity will be somewhat more complicated.

The relationship between the maximum heat flux and the mass flux is illustrated in Fig. 2 for several different liquid/material combinations. To determine the accuracy of this analytical solution, experimental data from the investigation of Stroes et al.[9] are also illustrated. Although these data were obtained for thin liquid films on flat copper plates, the thickness of the thin film and the radius of the grooves utilized in this solution are comparable, making it acceptable for comparison. As illustrated, the experimentally obtained rewetting heat flux values for R-113 and denatured alcohol films on copper plates are in reasonably good agreement with the theoretical values obtained using Eq. (12). However, as the mass flux becomes larger, the difference between the measured and predicted values diverge significantly.

Conclusion

A physical model has been developed and a theoretical investigation conducted to determine the rewetting characteristics of thin liquid films flowing over a flat grooved plate. An expression for the rewetting velocity as a function of the thermal properties of the liquid and the plate, the input heat flux to the plate, and the groove radius has been derived analytically. The analytically predicted maximum heat flux as a function of the mass flux has been compared with the experimental data of other investigators and shown to agree reasonably well at low mass flux levels. The theoretical analyses presented here also demonstrates the effects of variations in the geometry and structure on rewetting, and supports the conclusions proposed by several other investigators who have studied the effect of wick structures on rewetting in high capacity heat pipes.

The resulting expressions for predicting the rewetting conditions and limits will aid in the design of many types of heat exchangers, and also in the design of the evaporator portion of heat pipes designed for use on future spacecraft. Finally, additional experimental investigations are required to evaluate further the validity of the theoretical analyses presented here.

References

[1]Shires, G. L., Pickering, A. R., and Blacker, P. T., "Film Cooling of Vertical Fuel Rods," Rept. AEEW-R343, Atomic Energy Establishment, Winfrith, England, 1964.

[2]Elliott, D. F., and Rose, P. W., "The Quenching of a Heated Surface by a Film of Water in a Steam Environment at Pressures up to 53 Bar," Rept. AEEW-M976, Atomic Energy Establishment, Winfrith, England, 1970.

[3]Kalinin, E. K., "Investigation of the Crisis of Film Boiling in Channels," *Proceedings of the Two-Phase Flow and Heat Transfer in Rod Bundles Symposium*, ASME Winter Annual Meeting, Los Angeles, CA, 1969.

[4]Iloeje, O. C., Plummer, D. N., Rohsenow, W. N., and Griffith, P., "Effects of Mass Flux, Flow Quality, Thermal and Surface Properties of Materials on Rewet of Dispersed Flow Film Boiling," *Journal of Heat Transfer*, Vol. 104, No. 2, 1982, pp. 304–308.

[5]Ueda, T., Inoue, M., Iwata, Y., and Sogawa, Y., "Rewetting of a Hot Surface by a Falling Liquid Film," *International Journal of Heat and Mass Transfer*, Vol. 14, No. 2, 1971, pp. 401–410.

[6]Ueda, T., Tsunenori, S., and Koyanagi, M., "An Investigation of Critical Heat Flux and Surface Rewet in Flow Boiling Systems," *International Journal of Heat and Mass Transfer*, Vol. 26, No. 8, 1983, pp. 1189–1198.

[7]Bankoff, S. G., "Stability of Liquid Flow Down a Heated Inclined Plane," *International Journal of Heat and Mass Transfer*, Vol. 14, No. 2, 1971, pp. 377–385.

[8]Orell, A., and Bankoff, S. G., "Formation of a Dry Spot in a Liquid Film Heated from Below," *International Journal of Heat and Mass Transfer*, Vol. 14, No. 5, 1971, pp. 1838–1842.

[9]Stroes, G., Fricker, D., Issacci, F., and Catton, I., "Heat Flux Induced Dryout and Rewet in Thin Films," *Proceedings of the Ninth International Heat Transfer Conference*, Vol. 6, 1990, pp. 359–364.

[10]Bankoff, S. G., "Dynamics and Stability of Thin Heated Liquid Films," *Journal of Heat Transfer*, Vol. 112, No. 3, 1990, pp. 538–546.

Flowfield Analysis for High-Enthalpy Arc Heaters

Frank S. Milos*
NASA Ames Research Center,
Moffett Field, California 94035

Introduction

FOR more than two decades, electric arc jets have provided heat-transfer simulations of hypersonic flight en-

Received April 9, 1991; presented as Paper 91-1384 at the AIAA 26th Thermophysics Conference, Honolulu, HI, June 24–26, 1991; revision received Oct. 7, 1991; accepted for publication Oct. 10, 1991.

*Computational Aerothermodynamicist, Thermal Protection Materials Branch and Arc Jet Research Office. Member AIAA.

vironments.[1-6] The segmented, constricted arc-heater design has been particularly successful for long-duration simulations at low-to-moderate pressures required for hypersonic (nonballistic) reentry flight conditions.[3-6] Two such arc heaters are actively used at the NASA Ames Research Center. The 20 MW Aerodynamic Heating Facility and the 60 MW Interaction Heating Facility provide peak enthalpies of 30 MJ/kg and 46 MJ/kg, respectively, for simulation of the aerothermal heating pulse on the Space Shuttle[4] and the aeroassisted orbital transfer vehicle (AOTV).[6]

The next generation of spacecraft will undoubtedly employ aerobraking maneuvers to produce the required velocity decrement for fast lunar or interplanetary return to earth. Heating simulations for these missions require enthalpies significantly greater than can be obtained in existing facilities, on the order of 70–90 MJ/kg or higher. This note is an initial study of the feasibility, nominal geometry, and operating conditions for design of a constricted arc heater to provide such high enthalpy levels.

In this work, the ARCFLO (arc heater flowfield) computer program[7-9] is used to analyze the flow in the constrictor tube, which is the most critical portion of the flowfield. The ARCFLO code is modified for improved accuracy in high-enthalpy, radiation-dominated flows. The ARCFLO band-radiation model is compared with the state-of-the-art spectral-radiation code NEQAIR (nonequilibrium air radiation),[10-11] and the band-absorption coefficients are modified to match the overall radiative power. Parametric studies are then performed to determine the arc heater geometry and operating conditions consistent with existing hardware capabilities and limitations.

Comparison of Radiation Models

In a segmented arc heater at high enthalpies, radiation becomes the dominant heat-transfer mechanism. Flowfield calculations must use a reliable radiation model to make credible predictions of arc heater performance. In order to assess the accuracy of the ARCFLO radiation model, detailed comparisons are made between predictions of the ARCFLO and NEQAIR radiation models for the pressure and temperature ranges of interest in this work.

The NEQAIR code, developed by Park,[10] calculates detailed spectral (line-by-line) emission and absorption for air given the equilibrium or nonequilibrium thermodynamic state information at any point. A typical calculation uses 140,000 wavelengths between 100 and 2,000 nm. The ARCFLO code, on the other hand, contains a two-band grey-gas model for equilibrium air with band-absorption coefficients tabulated as functions of temperature and pressure. ARCFLO also contains subroutines that calculate the radiative flux in cylindrical geometry. Axial variations in properties are neglected (a "tangent annulus" approximation) so that the radiative flux can be determined from the temperature and absorption-coefficient profiles across the constrictor at each axial location.

To compare predictions from the two radiation models, pressure and temperature profiles are prescribed across the constrictor diameter. Equilibrium species concentrations for air are calculated using the chemistry code of Liu and Vinokur.[12] The NEQAIR code is run for each radial node to obtain the spectral absorption coefficient as a function of radial location, and the radiative flux in a cylinder is determined using modified versions of the radiation subroutines from ARCFLO. Code modifications include correction of wavelength and radial integration errors. The results of these calculations are compared with ARCFLO band-radiation calculations using the same pressure and temperature profiles.

For this analysis, the pressure was a constant value between 1 and 10 atm. Realistic temperature profiles vary in shape from approximately parabolic to very flat with a thin boundary layer near the wall. At high current density the profiles are relatively flat. The peak centerline temperature ranges from 12,000 K to 20,000 K or higher.

Figure 1 presents typical results from the two models for a pressure of 5 atm and a representative temperature profile with peak temperature of 14500 K and wall temperature of 1000 K. The spectral flux (spectral power per unit area) incident on the constrictor wall is plotted as a function of the photon energy in electron volts (EV). The NEQAIR data have been smoothed over 1/2 EV bands. The ARCFLO model predicts total radiative wall heating of 12.8 kW/cm^2, primarily in the band below 10.5 EV (above 118 nm); whereas, the NEQAIR model predicts total radiative heating of 7.3 kW/cm^2 in a spectral distribution with significant contributions from ultraviolet and infrared lines, but little contribution from 3–7 EV.

The same calculations were performed for different temperature profiles and pressures up to 10 atm. The results, summarized in Fig. 2, show a range of radiative power for each code, depending on flatness of the assigned temperature profile. In the operating range of interest, below 10 atm, ARCFLO overestimates the heat transfer compared with NEQAIR. This is a very critical difference, because the ARCFLO results exceed at much lower pressure the existing design limit of approximately 12 kW/cm^2 for continuous arc-heater operation.

The ARCFLO predictions can be lowered into better agreement with the NEQAIR results by reducing the band-absorption coefficients. The original coefficients were multiplied by a linear function of temperature. A good agreement with the NEQAIR predictions was obtained when the original values were reduced by up to 40% at high temperatures. Figure 3 illustrates ARCFLO results for average total enthalpy and total wall heating as functions of axial location for the unmodified ARCFLO radiation model and for the new model with reduced absorption coefficients. The maximum heating occurs near the constrictor inlet where the centerline temperature is high (above 20,000 K). The peak heating is nearly 14 kW/cm^2 for the original model, but below 11 kW/cm^2 using the modified radiation model. The enthalpy is also higher in the latter case, because the constrictor column operates more efficiently when radiation losses are reduced. Of course, the higher enthalpy gas has higher temperature, so the reduction in wall heating is less than indicated by Fig. 2. The modified

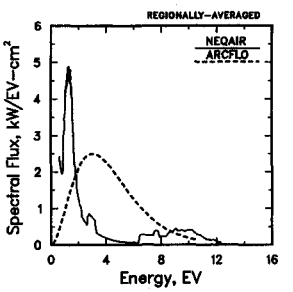

Fig. 1 Spectral flux at constrictor wall predicted by ARCFLO and NEQAIR radiation models for assigned temperature profile; 6-cm diam and 5-atm pressure. The NEQAIR results are smoothed over 1/2 EV bands.

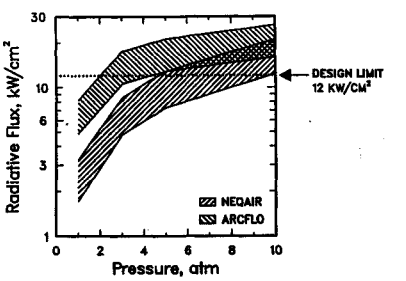

Fig. 2 Total radiative flux at constrictor wall predicted by ARCFLO and NEQAIR radiation models for assigned pressure and temperature profiles; 6-cm diam.

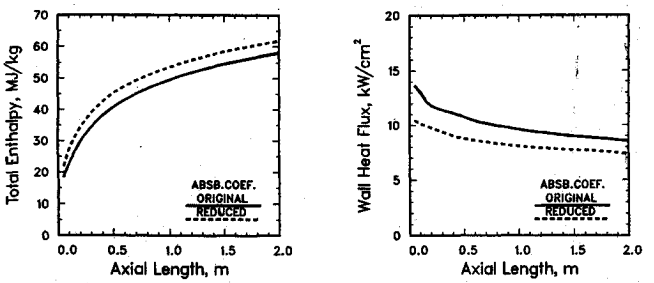

Fig. 3 ARCFLO results for axial distribution of average enthalpy and wall heating; 6-cm diam, 5-atm pressure, 17,000 A, and 0.25 kg/s flow rate. Comparison of original ARCFLO model with reduced-absorption-coefficient model.

two-band radiation model was used for all calculations presented in the next section.

ARCFLO Parametric Studies

The goals of this parametric study are to determine the nominal geometry and operating conditions for a next-generation segmented arc heater with enthalpies in the range of 70–90 MJ/kg. This enthalpy range is selected to match conditions for the heating pulse during aerobraking reentry from the moon or from Mars. The flow rate is to be maximized to enable the use of larger model sizes and to avoid rarified-flow effects in the test chamber. However, with existing hardware limitations, the maximum wall heat transfer rate must stay below about 12 kW/cm² to provide a small safety margin against possible constrictor melt-down. In addition, the total power consumption is limited to 300 MW and the total current to 20,000 A.

The parametric studies have five operational parameters: constrictor diameter; constrictor length; arc current; stagnation pressure; and flow rate. However, the latter two are not independent if the nozzle throat diameter or area ratio are specified. The dependent variables are the results of the calculations, which include arc-heater performance variables such as voltage, average outflow enthalpy, and peak wall heating.

The calculations are performed with a modified version[9] of the ARCFLO code and the radiation model corrections described in the previous section. The air injection is distributed along the length of the column, because this method of injection has been found to produce stable flow below 10 atm and to reduce the possibility of voltage breakdown between constrictor disks.

Several hundred ARCFLO calculations were made. The dependent variables are found to be strong functions of pressure, diameter, and current. For fixed values of the latter three parameters, the peak wall heating is relatively insensitive to constrictor length and flow rate, the outflow enthalpy increases with constrictor length and flow rate, and the voltage increases approximately linearly with constrictor length. To maximize the enthalpy, it is advantageous to use a long constrictor, preferably with a length-to-diameter ratio of 30 or more, and to operate at flow rates just below the choking value. The most promising results were obtained for 5-cm- and 6-cm-diam constrictors.

Figure 4 summarizes results for a 5 × 200 cm constrictor. Plotted are the average total enthalpy at the constrictor outlet and the range of maximum wall heat transfer for three operating pressures and for varying arc current. For each pressure, the flow rate is just below the choking value. The wall heating is essentially all radiative and increases with both pressure and current. The enthalpy increases with current but decreases with increasing pressure, owing to the strong pressure dependence of radiative losses (cf. Fig. 2). At 5 atm and 0.175 kg/s, the heat transfer limit (12 kW/cm²) is clearly exceeded at 14,000 amp, but the enthalpy is below 63 MJ/kg. However, at 3 atm and 0.1 kg/s, the constrictor can operate around 14,000–15,000 A and reach the low end of the desired enthalpy range, 70–75 MJ/kg. At 2 atm and 17,000 A, the

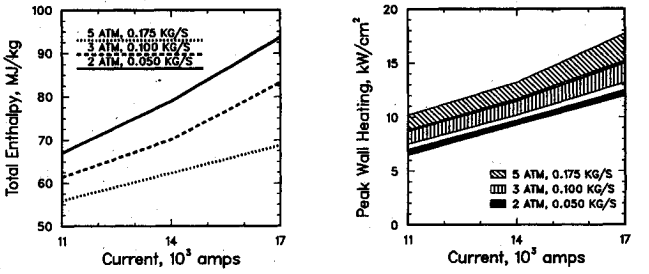

Fig. 4 Average outflow enthalpy and peak heating range for 5 × 200 cm constrictor.

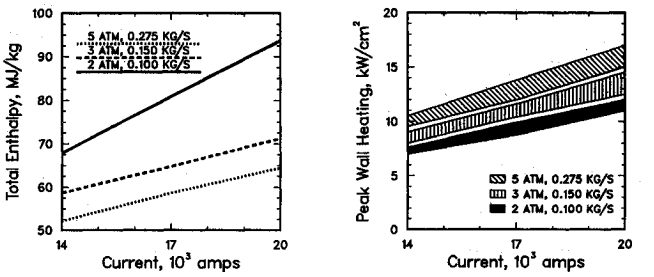

Fig. 5 Average outflow enthalpy and peak heating range for 6 × 200 cm constrictor.

column can (barely) reach 90 MJ/kg, but the flow rate is only 0.05 kg/s. The total power consumption is under 70 MW for all cases.

Results similar to the above were obtained for other constrictor diameters. Figure 5 summarizes results for a 6 × 200 cm constrictor. At 5 atm and 0.275 kg/s, the column must operate below 16,000 amp, but the enthalpy is below 56 MJ/kg. At 3 atm, 0.15 kg/s, and 19,000 A the heating is too high, and the enthalpy is below 70 MJ/kg. However, operation at 2 atm and 0.1 kg/s is safe up to 20,000 A and produces enthalpies up to 90 MJ/kg in the constrictor. The total power consumption is under 100 MW. Therefore, the 6-cm constrictor can reach the highest enthalpies at higher flow rates than the 5-cm constrictor, but at the cost of increased current and power. Constrictors with diameters larger than 6 cm require more than 20,000 A of current to produce comparable high enthalpies and flow rates.

Concluding Remarks

The design goals of high enthalpy and high flow rate are contradictory. High enthalpy is best achieved by lowering the pressure, because radiation losses decrease and the constrictor operates most efficiently at low pressures. However, high flow rate is achieved by increasing the pressure or diameter, and increasing the latter raises the current and power requirements.

Power consumption is below 100 MW for all cases considered in this study. If 300 MW of power are available, the total flow rate may be increased by combining the flow from multiple constrictors. However, flow quality then becomes an issue.

Constrictor wall cooling is the most critical design limitation for the next generation of high-enthalpy, segmented arc heaters. Significant increases in arc-heater flow rate and enthalpy are possible if the constrictor disk heat-transfer capability is increased, possibly through disk redesign or the use of more conductive materials.

The parametric studies indicate that arc currents of 14,000–20,000 A are required to reach enthalpies of 70–90 MJ/kg. However, it must be noted that the highest arc current run to date is 6500 A in the 60 MW Interaction Heating Facility.[6] The high current requirement raises a number of issues not addressed in this work, including safety, operational procedures, and electrode design, stability, and flowfield analysis. These issues are currently being studied.

References

[1]Vorreiter, J. W., and Shepard, C. E., "Performance Characteristics of the Constricted-Arc Supersonic Jet," *Proceedings of the Heat Transfer and Fluid Mechanics Institute*, edited by A. F. Charwat, Stanford Univ., Stanford, CA, June 1965, pp. 42–49.

[2]Shepard, C. E., Watson, V. R., and Stine, H. A., "Evaluation of a Constricted-Arc Supersonic Jet," NASA TN D-2066, Jan. 1964.

[3]Shepard, C. E., Ketner, D. M., and Vorreiter, J. W., "A High-Enthalpy Plasma Generator for Entry Heating Simulation," NASA TN D-4583, May 1968.

[4]Winovich, W., and Carlson, W. C. A., "The 60-MW Shuttle Interaction Heating Facility," *Proceedings of the 25th International Instrumentation Symposium*, Instrument Society of America, Pittsburg, PA, May 1979, pp. 59–75.

[5]Winovich, W., and Carlson, W. C. A., "The Giant Planet Facility," presented at the 25th International Instrumentation Symposium, Anaheim, CA, May 1979.

[6]Winovich, W., Balboni, J., and Balakrishnan, A., "Application of Numerical Simulation to Enhance Arcjet Performance Simulation," *Thermophysical Aspects of Reentry Flows*, edited by J. N. Moss and C. D. Scott, Vol. 103, Progress in Aeronautics and Astronautics, AIAA, New York, 1986, pp. 393–415.

[7]Watson, V. R., and Pegot, E. B., "Numerical Calculations for the Characteristics of a Gas Flowing Axially Through a Constricted Arc," NASA TN D-4042, June 1967.

[8]Nicolet, W. E., Shepard, C. E., Clark, K. J., Balakrishnan, A., Kesselring, J. P., Suchsland, K. E., and Reese, J. J., "Methods for the Analysis of High-Pressure, High-Enthalpy Arc Heaters," AIAA Paper 75-704, Denver, CO, May 1975.

[9]Nicolet, W. E., Shepard, C. E., Clark, K. J., Balakrishnan, A., Kesselring, J. P., Suchsland, K. E., and Reese, J. J., "Analytical and Design Study for a High-Pressure, High-Enthalpy Constricted Arc Heater," Arnold Engineering Development Center, TR-75-47, July 1975.

[10]Park, C., "Calculation of Nonequilibrium Radiation in the Flight Regimes of Aeroassisted Orbital Transfer Vehicles," *Thermal Design of Aeroassisted Orbital Transfer Vehicles*, edited by H. F. Nelson, Vol. 96, Progress in Astronautics and Aeronautics, AIAA, New York, 1985, pp. 395–418.

[11]Park, C., "Nonequilibrium Air Radiation (NEQAIR) Program: User's Manual," NASA TM 86707, July 1985.

[12]Liu, Y., and Vinokur, M., "Equilibrium Gas Flow Computations. Part 1: Accurate and Efficient Calculation of Equilibrium Gas Properties," AIAA Paper 89-1736, Buffalo, NY, June 1989.

Source Function Approach for Radiative Heat Transfer Analysis

J. Huan* and M. H. N. Naraghi†

Manhattan College, Riverdale, New York 10471

Introduction

THIS note presents a source function approach for analysis of three-dimensional radiative heat transfer in absorbing, emitting, and anisotropically scattering media. Two integral equations relating the source function for the gas and leaving intensity for surfaces are developed incorporating direct exchange factors between differential elements. The resulting equations are then discretized using a numerical scheme. Numerical results based on the present approach are presented for a three-dimensional idealized furnace model, which are in excellent agreement with the existing solutions.

Received April 5, 1991; revision received Oct. 28, 1991; accepted for publication Nov. 1, 1991.

*Graduate Assistant, Department of Mechanical Engineering.

†Associate Professor, Department of Mechanical Engineering. Member AIAA.

Formulation

Consider a multidimensional diffuse boundary enclosure containing absorbing, emitting, and anisotropically scattering media, as shown in Fig. 1. Neglecting the conductive and convective heat transfer effects, the following integral equations can be derived for radiative heat transfer in the enclosure (see Ref. 1 for derivations)

$$I_s(\mathbf{r}) = \varepsilon i_{bs}(\mathbf{r}) + \frac{\rho}{\pi}\int_{2\pi} I_s(\mathbf{r}')\tau(|\mathbf{r}-\mathbf{r}'|)\cos\theta_r\, d\Omega' + \frac{\rho}{\pi}\int_{2\pi}\int_0^{|r-r'|} I_g(\mathbf{r}_l,\Omega')\tau(|\mathbf{r}-\mathbf{r}_l|)\cos\theta_r K_t\, dl\, d\Omega' \quad (1)$$

$$I_g(\mathbf{r},\Omega) = \frac{q_g'''(\mathbf{r})}{4\pi K_t} + \frac{1}{4\pi}\int_{4\pi} I_s(\mathbf{r}')\tau(|\mathbf{r}-\mathbf{r}'|)\times[\omega_0\Phi(\Omega',\Omega)-\omega_0+1]\,d\Omega' + \frac{1}{4\pi}\int_{4\pi}\int_0^{|r-r'|} I_g(\mathbf{r}_l,\Omega')\tau(|\mathbf{r}-\mathbf{r}_l|)\cdot[\omega_0\Phi(\Omega',\Omega)-\omega_0+1]K_t\, dl\, d\Omega' \quad (2)$$

$$q_s''(\mathbf{r}) = \varepsilon E_{bs}(\mathbf{r}) - \varepsilon\int_{2\pi} I_s(\mathbf{r}')\tau(|\mathbf{r}-\mathbf{r}'|)\cos\theta_r\, d\Omega' - \varepsilon\int_{2\pi}\int_0^{|r-r'|} I_g(\mathbf{r}_l,\Omega')\tau(|\mathbf{r}-\mathbf{r}_l|)\cos\theta_r K_t\, dl\, d\Omega' \quad (3)$$

$$4(1-\omega_0)E_{bg}(\mathbf{r}) = \frac{q_g'''(\mathbf{r})}{K_t} + (1-\omega_0)\int_{4\pi} I_s(\mathbf{r}')\tau(|\mathbf{r}-\mathbf{r}'|)\,d\Omega' + (1+\omega_0)\int_{4\pi}\int_0^{|r-r'|} I_g(\mathbf{r}_l,\Omega')\tau(|\mathbf{r}-\mathbf{r}_l|)K_t\, dl\, d\Omega' \quad (4)$$

where $\mathbf{r}_l = \mathbf{r}' + l(\mathbf{r}-\mathbf{r}')/|\mathbf{r}-\mathbf{r}'|$, $\tau(|\mathbf{r}-\mathbf{r}'|) = \exp(-K_t|\mathbf{r}-\mathbf{r}'|)$ is the transmittance between location $\mathbf{r}$ and $\mathbf{r}'$, I_g is

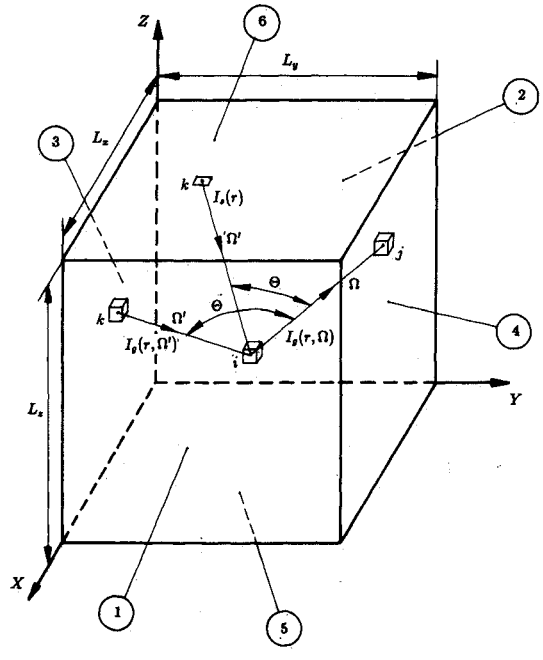

Fig. 1 Schematic of a three-dimensional rectangular enclosure.